nature methods

Review article

https://doi.org/10.1038/s41592-025-02935-5

Methods to analyze cell migration data: fundamentals and practical guidelines

Received: 7 January 2025

Accepted: 13 August 2025

Published online: 18 December 2025

Check for updates

Pei-Hsun Wu[1,2,7] ✉, Jude M. Phillip[1,2,3,4,5,7] ✉, Wenxuan Du[1,2], Andre Forjaz[1,2], Praful R. Nair[1,2] & Denis Wirtz[1,2,5,6] ✉

Cell migration assays provide invaluable insights into fundamental biological processes. In a companion Review, we describe commercial and custom in vitro and in vivo assays to measure cell migration and provide guidelines on how to select the most appropriate assay for a given biological question. Here, we describe the fundamental principles of how to compute—from the raw data generated by these assays—quantitative cell migration parameters that help determine the biophysical nature of the cell migration, such as cell speed, mean-squared displacement, diffusivity, persistence, speed and anisotropy, and how to quantify cell heterogeneity, with practical guidance. We also describe new imaging and computational technologies, including AI-based methods, which have helped establish fast, robust and accurate tracking of cells and quantification of cell migration. Taken together, these Reviews offer practical guidance for cell migration assays from conception to analysis.

Migration is a fundamental cellular process that regulates a wide variety of biological processes, including immune surveillance and responses[1,2], embryonic development[3–5] and wound healing[6–9]. The onset and dysregulation of cell migration can lead to adverse outcomes and diseases, such as metastatic spread of cancer cells to distant organs and pro-inflammatory dysfunctions[10–15]. Studying the biophysical principles and molecular pathways that drive cell migration in healthy and diseased contexts has helped uncover potential therapeutic targets[16–18]. In recent decades, numerous cell migration assays have emerged to investigate the principles and regulators of cell movements in diverse biological scenarios. In a companion paper[19], we describe in depth commercial and custom in vitro and in vivo assays to measure cell migration. In that paper, we provide guidelines on how to select the most appropriate assay for a given biological question, based on rigorous criteria of biological mimicking, cost, ease of implementation, productive capacity, necessity of live-cell microscopy, amenability to post-assay downstream molecular analysis, ability to quantify cell heterogeneity and number of cells needed to run each assay.

Here, we describe the fundamental principles and practical guidelines of how to compute—from the raw data generated by these assays—cell migration parameters, such as cell speed, mean-squared displacement (MSD), diffusivity, persistence, speed, anisotropy, and so on, and how to quantify cell heterogeneity. These parameters help determine the biophysical nature of the cell migration under study and potential molecular mechanisms of regulation. Thanks to the recent introduction of new imaging and computational technologies, various analytical and computational methods, including AI-based methods, have been established for fast, robust and accurate tracking of cells and quantification of cell migration, which we review below.

Direct-versus-indirect cell migration measurements

Cell migration measurements fall into two main categories: direct and indirect (Fig. 1). Direct-migration measurements involve tracking the real-time movements of individual cells via video-based microscopy, providing the time-dependent coordinates $(x(t), y(t), z(t))$ that describe

[1]Department of Chemical & Biomolecular Engineering, Johns Hopkins University, Baltimore, MD, USA. [2]Institute for NanoBioTechnology, Johns Hopkins University, Baltimore, MD, USA. [3]Department of Biomedical Engineering, Johns Hopkins University, Baltimore, MD, USA. [4]Translational Therapeutics and Regenerative Engineering Center, Johns Hopkins University, Baltimore, MD, USA. [5]Department of Oncology, Johns Hopkins School of Medicine, Johns Hopkins University, Baltimore, MD, USA. [6]Department of Pathology, Johns Hopkins School of Medicine, Johns Hopkins University, Baltimore, MD, USA. [7]These authors contributed equally: Pei-Hsun Wu, Jude M. Phillip. ✉e-mail: pwu@jhu.edu; jphillip@jhu.edu; wirtz@jhu.edu

https://doi.org/10.1038/s41592-025-02935-5

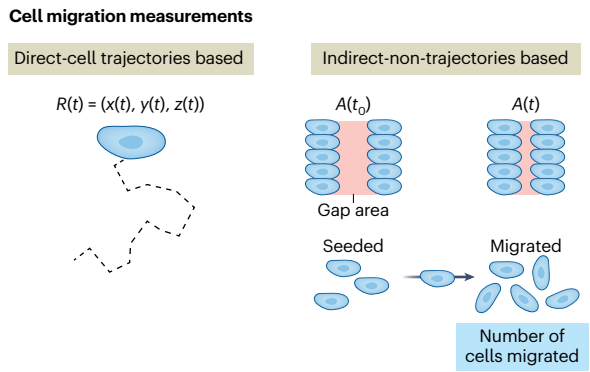

Fig. 1 | Direct-versus-indirect measurements of cell migration. Direct measurements entail the tracking of individual cells during their migration, from which migration parameters such as speed and MSD for individual cells can be computed. Indirect measurements entail an end-point measurement as a proxy of cell migration (see text and companion Review[19]). Direct measurements include the 2D and 3D cell migration assays and the microslide chemotaxis assay. Indirect measurements include the Transwell assay, as well as the standard wound-healing assay, spheroid and confined migration assays. The wound healing, spheroid and confined migration assays can be transformed into direct measurements if tracking of individual cells in these systems is feasible.

the trajectories of each tracked cell. Measurements and analysis of cell trajectories acknowledge the heterogeneity of cells, even clonal cells, and offer a wealth of information that reflects underlying complex biological programs and can help reveal sometimes subtle, but important differences between biological conditions that modulate migration phenotypes not well described by averages[20–24]. In addition to conventional migration parameters such as average speed, which can be directly computed from trajectories, statistical profiling of the cell trajectories and various mathematical models such as the persistence random walk[21,25–27] can be used to gain deeper mechanistic insights into cell migration (Fig. 2 and Supplementary Table 1).

In contrast to direct measurements, indirect migration measurements refer to assessments that do not involve direct tracking of individual cells (Fig. 1). Indirect migration measurements gauge properties that correlate with and produce proxies of cell migration. Indirect measurements result from end-point experiments, that is, they analyze a snapshot of cells obtained at the end of a time-dependent migratory process (see companion Review[19]). For instance, in the Transwell migration assay, the extent of cell migration through a porous membrane is indirectly estimated by counting the number of cells that traversed the membrane after a defined time period[28,29]. Such end-point measurements do not provide mechanistic insight on how the cells physically migrate through the membrane. However, since live-cell microscopy is not required, end-point measurements tend to be more readily accessible to laboratories without specialized equipment, such as time-lapsed fluorescence and intravital two-photon microscopes.

Indirect migration measurements tend to be more scalable than direct measurements. This scalability allows users to conduct migration assessments of a large number of samples and conditions for applications such as high-throughput CRISPR-based screens and testing of potential migration inhibitors that may regulate cell migration[30,31]. Importantly for indirect end-point measurements, cell migration assessments can be influenced by cell proliferation[32]. Measuring and comparing motility under conditions with notably different proliferation rates should be approached with caution. Pharmacological inhibition or serum starvation can help control cell growth; however, these treatments can also have profound and complex effects on cell migration itself, which should be carefully considered when analyzing cell migration data[33]. Although many assays have been traditionally performed as indirect measurements—such as the two-dimensional (2D) wound-healing assay—the advent of new imaging technologies has prompted researchers to create live-cell versions of these assays to acquire richer time-resolved datasets[34,35] (Fig. 1).

In the following sections, we describe how direct and indirect measurements of cell migration are analyzed, outline analytical considerations specific to each assay, and review recent developments in the analysis of large cell migration datasets.

Analysis of direct cell migration measurements

For direct cell migration measurements, the movements of cells are typically recorded in the form of a video via time-lapsed light microscopy. Direct-migration measurements have been (or could) be implemented in the following assays described in the companion Review[19]: The wound-healing assay, the 2D/three-dimensional (3D) cell migration assay, the spheroid/organoid invasion assay, the confined migration assay and migration on 2D micropatterns. Direct-migration analysis consists of two main components: (1) the detection and tracking of the time-dependent locations of cells from the acquired time-lapsed videos and (2) the analysis of the resulting cell trajectories using analytical or stochastic models of cell migration.

Methods for cell tracking

Time-resolved trajectories of migrating cells are typically obtained from analysis of video-based cell imaging such as brightfield or fluorescence microscopy[36,37]. Extracting cell trajectories from videos remains a nontrivial task. Manual tracking is the most common approach to track cell locations in videos[36,38]: The user identifies a cell in the first frame of the video and registers its time-dependent locations in a series of sequential image frames. The user can keep track of the identity of cells in sequential frames and recognize live from dead cells by playing the video back and forth. But tracking cells manually could be subject to user bias and inconsistency. Hence, users should set predetermined rules to select the cells to be tracked to avoid or reduce bias. For instance, the user should set the minimum size of the objects to track (to avoid tracking cell debris), avoid tracking cells that undergo division during the video (unless this is the focus of the study; see also above)

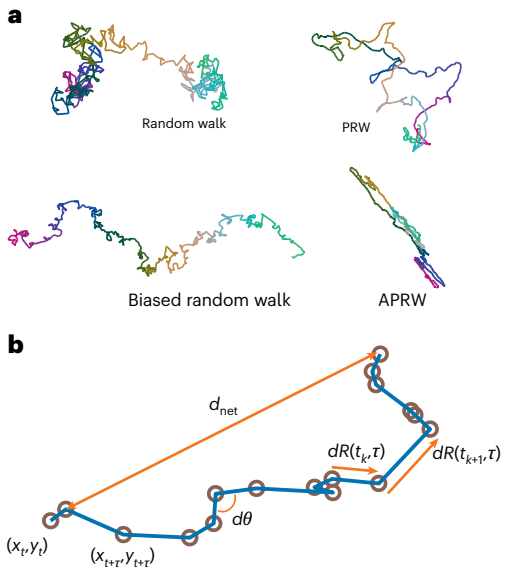

Fig. 2 | Characterization of cell trajectories and associated metrics. **a**, Examples of common modes of trajectories of migratory cells. A random walk represents a path where the direction of motion is chosen randomly at each step. The PRW introduces directional persistence, leading to smoother trajectories. A biased random walk includes a directional bias that influences the trajectory. The APRW combines both directional persistence and anisotropy, resulting in highly directed and elongated paths. **b**, Schematic representation of trajectory parameters and displacement metrics.

and cells that leave and reenter the field of view (to avoid issues of cell identification) and ensure the cells to be tracked are alive.

Manual tracking tends to be robust and applicable to videos derived from various imaging modalities, such as brightfield microscopy and phase-contrast or differential interference contrast microscopy for unlabeled cells and fluorescence microscopy for fluorescently labeled cells. Cells that are difficult to track, such as cells in noisy or poorly illuminated images, could still be tracked by adapting and modulating the intensity ranges or using features beyond strict image contrast parameters[39,40].

As migrating cells may cross paths with one another in consecutive frames, the frame rate in the video should be high enough to avoid confusion in the identification of tracked cells. The choice of an adequate frame rate depends on the extent of cell movements and the density of the cells in culture. In general, the distance traveled by cells between frames should be substantially lower than the average distance between neighboring cells. Tracking fast-moving cells such as monocytes and T cells requires a relatively high frame rate compared to tacking slower-moving cells, such as cancer cells and fibroblast cells[21] (see table of typical cell speeds in the companion Review[19]). Cell division may also occur during the tracking period, and dividing cells could exhibit different motility behavior compared to cells in interphase[38]. Hence, dividing cells should typically be excluded from the analysis, which can reduce the number of trackable cells. However, tools such as TrackMate[41] and CellTrackVis[42] have been developed for tracking cells with consideration of lineages and can be used to study cell migration associated with cell division or lineage.

Several free open-source and commercial software tools have been developed to assist in manual cell tracking, such as the manual object tracking module in MetaMorph[22,24] or the click-based tracking module of ImageJ/Fiji[43,44] (Table 1). Using such software, a trained researcher may take a few hours to track 100 cells in 100 consecutive frames. Therefore, the time required to probe, say, 20 different conditions (for example, 20 different gene perturbations or drugs) and track 100 cells per condition in biological triplicates, could take weeks. The limited throughput of manual tracking tools makes them tedious and unfeasible for analyzing large numbers of samples and cells. Additionally, user bias can influence the results. For instance, users may be biased toward tracking cells that move a lot across subsequent image frames or may tend to predominantly track cells that do not move much in efforts to maximize the number of tracked cells. Yet sampling a sufficiently high number of cells of varying migratory behaviors is critical to accurately define the distribution of cell migration phenotypes for a given fixed condition[45].

Semiautomated or automated cell tracking methods that utilize image processing or deep-learning-based algorithms have been developed to offer unbiased accurate tracking, resulting in much higher throughput than manual tracking. In fully automated cell tracking, cell trajectories can be extracted with little to no user input. In contrast, semiautomated cell tracking requires user-provided inputs, such as specified cell locations, for the program to process and track the cells. The general algorithms implemented for cell tracking are categorized into tracking by detection, model evolution and filtering[46]. The applicability of different methods for cell tracking is closely associated with the type of microscopy used (Table 1). One of the most common approaches to automatically track cell locations in sequential images is through cell segmentation, for which the cell locations are computed based on the geometric center of the segmented cells or their nuclei. Segmentation of fluorescently labeled cells offers high accuracy and is computationally less challenging compared to tracking label-free cells from brightfield images[47,48]. Software such as CellProfiler[48] can perform cell detection in fluorescence settings utilizing image processing pipelines (Table 1). Label-free cell tracking offers the benefit of a more streamlined sample preparation and minimal disturbance to cell physiology, since in many cases the addition of fluorophores can substantially influence cell behavior[49–51].

For brightfield images, accurately detecting the location of cells using traditional image processing approaches is generally more challenging than for fluorescence images, particularly under crowded conditions. The development of deep-learning convolutional neural networks offers solutions, which are revolutionizing the field of cell detection. Convolutional neural network frameworks are highly effective in performing segmentation tasks in various types of cell microscopy images, including grayscale images obtained with fluorescence or brightfield microscopy[52–54]. In particular, tools such as CellPose[52] and Meta's Track-Anything[55] can segment cells directly from brightfield and fluorescence images. Segmentation-based cell detection and tracking are particularly relevant for in vivo cell migration studies. Identifying single cells in vivo is often more challenging due to the densely packed environment of each cell, for which cell segmentation becomes essential to detect individual cells. Volumetric imaging is frequently used to account for structural variations in tissue structure[56–58]. Tools such as CellPose, IMARIS and 3DeeCellTracker have been developed for performing 3D cell segmentation and detection.[52,56]. The coordinates of cells tracked can further be compiled into time series or trajectories using packages, such as CellTracksColab, CelltrackR, TrackMateR, CellPhe, Traject3D and Cellplato (Table 1)[59–64].

The trajectories of cells can be obtained using other types of algorithms. For example, correlation-based algorithms have been used to identify displacements of selected cells in subsequent frames[24,55]. This type of analysis requires the selection of cell objects in the first image of a video to initiate tracking of the selected objects in the subsequent frames. A recent study shows that this type of method is highly accurate when tracking large objects[55]. Free and commercial software that provide cell tracking tools are provided in Table 1. In-depth reviews of cell tracking algorithms and methods can be found in refs. 37,46,55,65,66.

Once cell tracking is performed, quality control needs to be applied. For instance, the shift in the observation plane relative to the sample space may occur during experiments, leading to apparent convective movements of the tracked cells. Lack of appropriate correction for this apparent convection can lead to misinterpretation of the motility results. The shift can be removed through image registration before tracking or measuring the relative movement to a stagnant object (fiduciary marker) in the field of view[67]. Additionally, positioning accuracy relative to actual cell movement is a key factor to consider, as positioning errors can directly influence measured speed[25]. Large positioning errors lead to artificially high-speed measurements, particularly in (quasi)-immobile cells. Generally, positioning errors behave as white noise and do not depend on frame rate[68]. How their contribution to speed measurements can be assessed through the MSD profile over time is described in refs. 25,67–69.

Analysis of cell trajectories

The time-dependent coordinates of individual cells obtained via manual or automatic tracking of cells in videos constitute the inputs of analytical tools and pipelines that generate quantitative metrics of cell migration (Fig. 2 and Supplementary Table 1). Motility parameters are typically derived from ensemble-averaged measurements across tracking time and across all tracked cells for each experimental condition. A rolling window strategy has also been used to analyze motility data, and this type of analysis is particularly important for characterizing non-equilibrium states, where cell motility transitions over time[70–72].

Cell speed is the most straightforward and commonly used migration parameter that can be extracted directly from cell trajectories. However, eukaryotic cell migration is a complex and stochastic process[73–75]. Cells exhibit highly diverse patterns and modes of migration that tend to be different for different cell types and is context dependent based on microenvironmental cues (Fig. 2a). For example, cancer cells on a 2D matrix-coated substrate versus embedded inside a 3D matrix, such as collagen-I or Matrigel, exhibit fundamentally distinct modes of migration[21,25]. In addition, confluent cells in a monolayer

https://doi.org/10.1038/s41592-025-02935-5

Table 1 | Commercial and open-source software to track and analyze cell migration

Tool	Availability (source)	Applicable image type (imaging modalities)	Tracking algorithm	Platform
Commercial				
MetaMorph	Molecular Devices	Fluorescent, brightfield 2D/3D	Correlation-based template matching	Stand-alone
Imaris for Tracking	Oxford Instruments	Fluorescent, brightfield 2D/3D	Imaris 3D tracking algorithms	Stand-alone
Volocity	Quorum Technologies	Fluorescent 3D		Stand-alone
Arivis Pro (Vision4D)	ZEISS	Fluorescent, brightfield 2D/3D	AI-based segmentation	Stand-alone
Livecyte	Phasefocus	Fluorescent, brightfield 2D	Label-free segmentation	Stand-alone
BioTek Gen5	Agilent	Fluorescent, brightfield 2D	Segmentation	Stand-alone
Open source				
CellTrack[139]	http://db.cse.ohio-state.edu/CellTrack/	Fluorescent, brightfield 2D	Segmentation	Cross-platform
CellTracker[140]	https://github.com/WangLabTHU/CellTracker/	Fluorescent, brightfield 2D	Segmentation	Cross-platform
CellProfiler[48,141,142]	https://github.com/carpenterlab/2018_mcquin_PLOSBio/	Fluorescent, brightfield 2D/3D	Segmentation	Stand-alone
CellPose[52,143]	https://www.github.com/mouseland/cellpose/	Brightfield 2D/3D	Deep-learning-based segmentation	Cross-platform
MtrackJ[66]	https://imagescience.org/meijering/software/mtrackj/	Fluorescent, brightfield 2D/3D	Segmentation (manual)	ImageJ/Fiji
TrackMate[38,41]	https://github.com/trackmate-sc/TrackMate/	Fluorescent, brightfield 2D/3D	Segmentation (built-in or external)	ImageJ/Fiji
CellTrackVis[42]	https://github.com/scbeom/celltrackvis/	Brightfield 2D	Modeling via labeled random finite sets	Stand-alone
LIM Tracker[144]	https://github.com/LIMT34/LIM-Tracker/	Fluorescent, brightfield 2D	Deep-learning-based recognition	ImageJ/Fiji
DeLTA[145]	https://gitlab.com/delta-microscopy/delta/	Fluorescent, brightfield 2D	U-Net deep-learning segmentation	Cross-platform
HFM-Tracker[146]	https://pubs.rsc.org/en/content/articlelanding/2024/an/d4an00199k/	Brightfield 2D	CA-based detection ACM-based tracking	Cross-platform
AVeMap[147]	https://www.nature.com/articles/nmeth.2209#MOESM310/	Brightfield (wound healing) 2D	Correlation-based detection	MATLAB
TGMM[148]	https://www.janelia.org/lab/keller-lab/	Light-sheet 2D/3D	Gaussian Mixture Model	Cross-platform
iTrack4U[149]	https://journals.plos.org/plosone/article?id=10.1371/journal.pone.0081266#s3/	Fluorescent, brightfield 2D	Tracking input from other tools	Cross-platform
CelltrackR[63]	https://github.com/ingewortel/celltrackR/	Fluorescent two- photon imaging 2D/3D	Tracking input from other tools	R
CellMissy[150]	https://code.google.com/p/cellmissy/	Brightfield (wound healing) 2D	Tracking input from other tools	Cross-platform
3DeeCellTracker[56]	https://github.com/WenChentao/3DeeCellTracker/	Light-sheet 3D two-photon 3D spinning-disk confocal 3D	Deep-learning segmentation	Python (ImageJ for image alignment)
CellTracksColab[64]	https://github.com/CellMigrationLab/CellTracksColab/	Fluorescent, brightfield 2D	Tracking input from other tools	Cloud-based Google Colab or local-based Jupyter
Cellplato[60]	https://github.com/Michael-shannon/cellPLATO/	Fluorescent spinning-disk confocal 3D	Cellpose 2.0 -segmentation Btrack - tracking	Python
CellPhe[59]	https://zenodo.org/records/7620171#.ZAJZMuzP0o8/	Fluorescent, phase 2D	Phasefocus and TrackMate-Cellpose	R
Traject3D[61]	https://github.com/davebryantlab/Traject3d/	Label-free live-imaging (Incucyte) 2D/3D	Tracking input from CellProfiler	KNIME with R and Python integrations

exhibit collective migration behavior, which is also fundamentally different from the migration of cells far from one another[76–78]. Therefore, additional cell migration parameters have been derived from trajectories to capture the complex behavior of cells beyond cell speed, including the persistence time, the average turning angle and the total displacement of a cell. We summarize the common cell migration features that can be computed from cell trajectories in Fig. 2b and Supplementary Table 1. Due to the inherent stochastic nature of cell migration, several of these features, including instantaneous speed and angular displacement, depend on the imaging interval time that determines the time lag τ. Therefore, examining migration features at multiple time-lag reference points (typically shorter and longer than the persistence times of cells per condition) can provide a more comprehensive view of cell migration as opposed to a single time lag.

To derive a more comprehensive analysis of cell migration profiles, various statistical features of cell trajectories can be computed. These statistical features include the MSD, the autocorrelation function of cell velocities, the probability density function of cell displacements, the probability density function of angular displacements and the velocity polarization profile, to name a few[21] (see definitions in Supplementary Table 1). These statistical metrics provide a quantitative outlook of the strategy used by cells to migrate in a particular milieu. Particularly,

https://doi.org/10.1038/s41592-025-02935-5

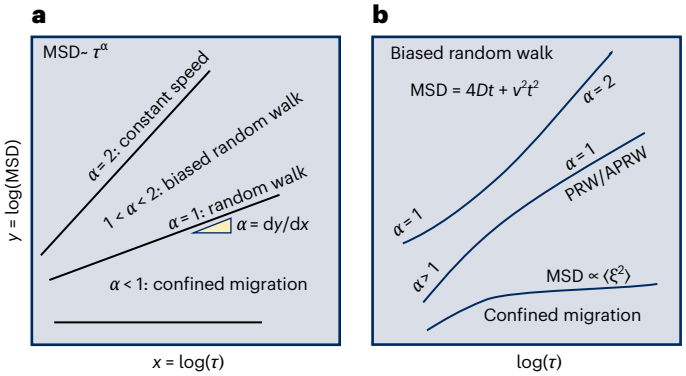

Fig. 3 | MSD for trajectory characterization. a, Log–log representation of the MSD as a function of time lag τ, showing different scaling behaviors. The characteristics of cell movement can be determined through exploring power-law relationship between MSD and time lag τ (that is, MSD ~ τ^{α}). The α can be computed from the slope of MSD profile at the logarithmic scale (that is, $\alpha = d\log(\mathrm{MSD})/d\log(\tau)$). For $\alpha = 2$, the trajectory corresponds to constant-speed motion. When $1 < \alpha < 2$, cell movements correspond to a biased random walk. A slope of $\alpha = 1$ corresponds to a standard random walk; $\alpha < 1$ suggests confined or restricted cell migration. **b**, Examples of migration models that exhibit complex, nonuniform MSD scaling profiles, including biased random walk, (anisotropic) persistent random walk and random migration of cells confined within a space of size. The MSD for a biased random walk exhibits α of 1 at a short time lag and α of 2 at a longer time lag. In PRW or APRW migration, migration is persistent at short time lag with $\alpha > 1$ and approximate free diffusion ($\alpha = 1$) at long time lags. If cell migration occurs within a confined space, α approaches 0 at long timescales, and the MSD value will correspond to the size of the confined space.

the MSD profile as a function of the time lag τ is essential to provide crucial information of cell migration processes, such as magnitude and mode of migration. The MSD of a cell migration is computed as shown in equation (1):

$$\mathrm{MSD}(\tau) = \langle (x(t+\tau) - x(t))^2 + (y(t+\tau) - y(t))^2 \rangle \quad (1)$$

Here, τ is the time lag, that is, the duration between images under consideration. $x(t)$ and $y(t)$ are the coordinates of the center of the cell, and $x(t+\tau)$ and $y(t+\tau)$ are the coordinates of the same cell at the time $t+\tau$, that is, a time lag τ later. If a video of migrating cells is collected for an hour at a frame rate of 20 frames per hour, then τ will vary between 0 min and 60 min at intervals of 3 min (60 min/20). The MSD profile is the time ensemble-averaged squared displacement of a cell at different time lags τ. The brackets $\langle \ldots \rangle$ signify the time-averaging operation. The MSD is directly related to cell speed v via $v(\tau) = \mathrm{MSD}(\tau)^{1/2}/\tau$.

How rapidly the MSD increases as a function of τ reflects how the cell migrates during the experiment, that is, whether the cell undergoes a random walk or a biased random walk, for instance (Fig. 3). A powerful way to quickly assess possible basic mechanisms of migration of a cell is to plot the MSD(τ) as a function of τ using a log–log plot and compute the exponent α by fitting the data to the following power law (Fig. 3) as shown in equation (2):

$$\mathrm{MSD}\,(\tau) \sim \tau^{\alpha} \quad (2)$$

For cell trajectories moving in a purely random work fashion, the MSD increases linearly with time lag and the exponent $\alpha = 1$. For cells undergoing biased migration, such as when cells are exposed to a chemotactic gradient, the exponent $\alpha > 1$. When the exponent $\alpha = 2$, the cell moves at a constant velocity v, where the MSD is expressed as $v^2\tau^2$. When the exponent $\alpha < 1$, cells exhibit confined/stalled motion. Thus, examining the statistical profiles of cells, such as MSD, can reveal valuable fundamental insights into their mode of migration (Fig. 3).

The migratory behavior of mammalian cells often exhibits more complex MSD profiles than those described by a universal time-lag scaling exponent[3,4,21,25,73,79]. The MSD exponent for cell migration can vary with time lag, influenced by factors such as noise from cell positioning errors, the inherently complex and stochastic nature of cell migration, constraints of the microenvironment (for example, cell–cell interactions and physical obstacles) or a combination of these factors[25,68,69]. Consequently, theoretical models have been developed to interpret these complex migration behaviors, as reviewed in the following sections.

Analyzing trajectory data using models of cell migration

Cell migration data can be interpreted through model-based analysis[21,73]. This approach aims to elucidate the complex and stochastic nature of cell trajectories using a small set of biologically or physically meaningful parameters derived from models of migration. In experiments that lack a symmetry-breaking gradient such as a chemoattractant source, both bacterial and eukaryotic cell motility are explained in terms of random-walk statistics. In particular, the persistent random walk (PRW) model is a stochastic model that has been extensively utilized to characterize eukaryotic cell migration on flat 2D substrates[25–27,80]. The PRW model describes the trajectory of cells as a succession of uncorrelated movements of duration larger than the persistence time P. The PRW model of cell migration is derived from the stochastic differential equation that describes the motion of a self-propelled cell as shown in equation (3):

$$\frac{dv}{dt} = -\frac{1}{P}v + \frac{S}{\sqrt{P}}\tilde{w} \quad (3)$$

where t is time, v is the cell velocity, P is the persistence time, S is the speed and $\tilde{w}$ is the vector of a so-called Weiner process[27]. The corresponding MSD of a cell undergoing a persistent random walk can be derived analytically (Fig. 2 and Supplementary Table 1) as shown in equation (4):

$$\mathrm{MSD}(\tau) = nS^2P^2\left(e^{-\frac{\tau}{P}} + \frac{\tau}{P} - 1\right) \quad (4)$$

Here, $n = 1$ for one-dimensional cell migration along linear tracks, $n = 2$ for 2D cell migration on a flat plane and $n = 3$ for 3D cell migration. The MSD can be used to extract persistence time P and speed S from the PRW model by fitting the experimental MSD derived from cell trajectories. 2D cell migration can often be effectively described with just these two parameters[25,26,80,81]. Importantly, while the observed MSD data can show a good fit to equation (4), this alone does not confirm that the migration under study follows a PRW model. For the PRW model to be valid, additional criteria must be satisfied, including a Gaussian distribution of velocities and a single-exponential decay of the velocity autocorrelation function, an isotropic velocity field and a uniform distribution of angles between cell movements at extended time scales[25] (Fig. 2 and Supplementary Table 1).

Recent studies have shown that cell migration often exhibits far more complex patterns than those described by the PRW model. Migration data from various cell types in 2D frequently reveal trends that deviate significantly from Gaussian distributions. For instance, non-Gaussian velocity distributions are commonly observed across different cell types and are associated with the microenvironment. To address these discrepancies, new models have been proposed to characterize cell migration[25,79,82–87]. For example, the migration of T cells in vivo is better characterized by Lévy flight statistics[86,87], exhibiting super-diffusive behavior across a wide range of time lags (that is, MSD(τ) ~ τ^{α} where $1 < \alpha < 2$) and consisting of sequences of numerous short steps interspersed with occasional longer 'flights'[87,88]. Recent studies suggest that the non-Gaussian velocity distribution can be explained under the PRW model for 2D migration[25].

Table 2 | Summary of computational tools for indirect measurements of cell migration across different assays

Assay type	Software	Source	Platform
Wound healing	CellProfiler[48,142]	https://cellprofiler.org/examples/	Python
Wound healing	Tscratch[151]	https://github.com/cselab/TScratch/	MATLAB
Wound healing	pyScratch[152]	https://github.com/ElsevierSoftwareX/PyScratch/	Python
Wound healing	MRI Wound Healing Tool	https://github.com/MontpellierRessourcesImagerie/imagej_macros_and_scripts/wiki/Wound-Healing-Tool/	ImageJ/Fiji
Wound healing	AIM[153]	https://www.mcbeng.it/en/category/software.html/	MATLAB
Transwell migration	CELLCOUNTER[154]	https://bitbucket.org/linora/cellcounter/downloads/	C++
Transwell migration	I-abACUS[155]	https://www.marilisacortesi.com/	MATLAB
Transwell migration	Cell Counter	https://imagej.net/plugins/cell-counter	ImageJ/Fiji
Spheroid	SpheroidSizer[156]	https://doi.org/10.3791/51639	MATLAB
Spheroid	AnaSP[157]	http://sourceforge.net/p/anasp/	MATLAB
Spheroid	SpheroScan[158]	https://github.com/FunctionalUrology/SpheroScan/	Python
Spheroid	OrgaExtractor[159]	https://github.com/tpark16/orgaextractor/	Python
Spheroid	OrganoID[160]	https://github.com/jono-m/OrganoID/	Python

When cells are embedded in a 3D matrix (for example, cancer cells migrating in a collagen-I matrix), their migration displays a high degree of anisotropy that is not described by the PRW model. As a result, a new model, the anisotropic random walk (APRW) model, was introduced, offering a more suitable characterization of 3D cell migration[25]. The APRW model is similar to the PRW model; however, cell migration is assumed to display different persistence and diffusivity along two orthogonal axes, the primary and secondary migration axes, in the observation plane (Fig. 2 and Supplementary Table 1). The primary and non-primary axes of cell migration are identified through principal component analysis (PCA) or singular vector decomposition on the cell velocity[21,25]. The MSD profiles calculated from the cell movement along the primary and non-primary axes can then be used to determine the persistence time and speed along both axes through equations (5) and (6):

$$\mathrm{MSD_p}(\tau) = S_\mathrm{p}^2 P_\mathrm{p}^2 \left(e^{-\frac{\tau}{P_\mathrm{p}}} + \frac{\tau}{P_\mathrm{p}} - 1 \right) \quad (5)$$

and

$$\mathrm{MSD_s}(\tau) = S_\mathrm{np}^2 P_\mathrm{np}^2 \left(e^{-\frac{\tau}{P_\mathrm{np}}} + \frac{\tau}{P_\mathrm{np}} - 1 \right) \quad (6)$$

The APRW model characterizes cell migration via the diffusivity, persistence time along the primary and secondary axes (D_p, D_np, P_p, P_np), as well as the total diffusivity D_tot and anisotropy index ϕ, computed as the ratio between the diffusivity of a cell in primary migration direction to non-primary directions (Fig. 2 and Supplementary Table 1). When there is no anisotropy in the system, $\phi = 1$, and the APRW model converges to the PRW model (Fig. 2 and Supplementary Table 1). The APRW model has been used to characterize the migration of various types of cells embedded in 3D collagen matrices, including monocytes, T cells and cancer cells, as well as cells embedded in composite 3D matrix systems[21,89–91].

Quantification of cell heterogeneity

Cells exhibit heterogeneous movement patterns in response to microenvironmental signals in the contexts of health and disease[92]. The traditional way to describe cell migration patterns for a tested condition is to track and analyze the movement of single cells and then report results as averages across all cells. From these pooled cell trajectories, one can compute migration parameters such as average speed, average persistence time and average total displacement. This approach of reporting cell migration data has led to important biological insights. However, recent advances in single-cell analyses are introducing new ways to measure and interpret cell migration patterns at single-cell resolution[45,60,72,93]. Instead of quantifying and reporting only bulk migration parameters, users can use single-cell analysis approaches that are similar to those used for single-cell sequencing. In these approaches, datasets are curated and harmonized—aligned across datasets to correct for imaging parameters, such as, spatial and temporal resolution, cell types, total imaging/analysis duration, and then migration parameters are computed per single cell[45]. Then using clustering analyses, including *k*-means, and unsupervised hierarchical clustering, and dimensional reduction techniques, including linear or nonlinear PCA, *t*-SNE[94] and UMAP[95], groups of cells with similar migration patterns are identified.

Using single-cell analysis to quantify cell migration presents advantages, including: (1) the ability to determine cell-to-cell variations (for instance, cellular heterogeneity can be determined based on Shannon entropy) across populations of cells and conditions; (2) visualization schemes that boost biological and statistical interpretability through high-dimensional clustering; (3) allowance for batch corrections and direct comparisons across multiple experiments and conditions within a high-dimensional data space; and (4) the ability to subcategorize cells across conditions, providing the ability to track emergent patterns that describe conserved or fractionally shifted cell populations[45].

Analysis of cell migration data obtained by common assays

Below we review and summarize the analytical tools and methods for both direct and indirect migration measurements that can be deployed for each assay described in the companion Review[19]. This overview focuses on the essential aspects of the analysis of the raw data generated by each assay described in our companion Review[19]. Software tools that can assist with the analysis of these indirect migration assays are summarized in Table 2. The 2D/3D migration assay and the µ-slide chemotaxis assay primarily measure cell migration directly. Hence, the analysis of the associated data will not be further reviewed in the following sections.

The wound-healing assay (scratch assay)

In the wound-healing assay, how rapidly cells move to fill the 'wounded' space is assessed to evaluate cell migration behavior and performance (Fig. 4). In this assay, the cells undergo transient (biased) migration patterns, and measuring the reduction of cell-free area or speed of

https://doi.org/10.1038/s41592-025-02935-5

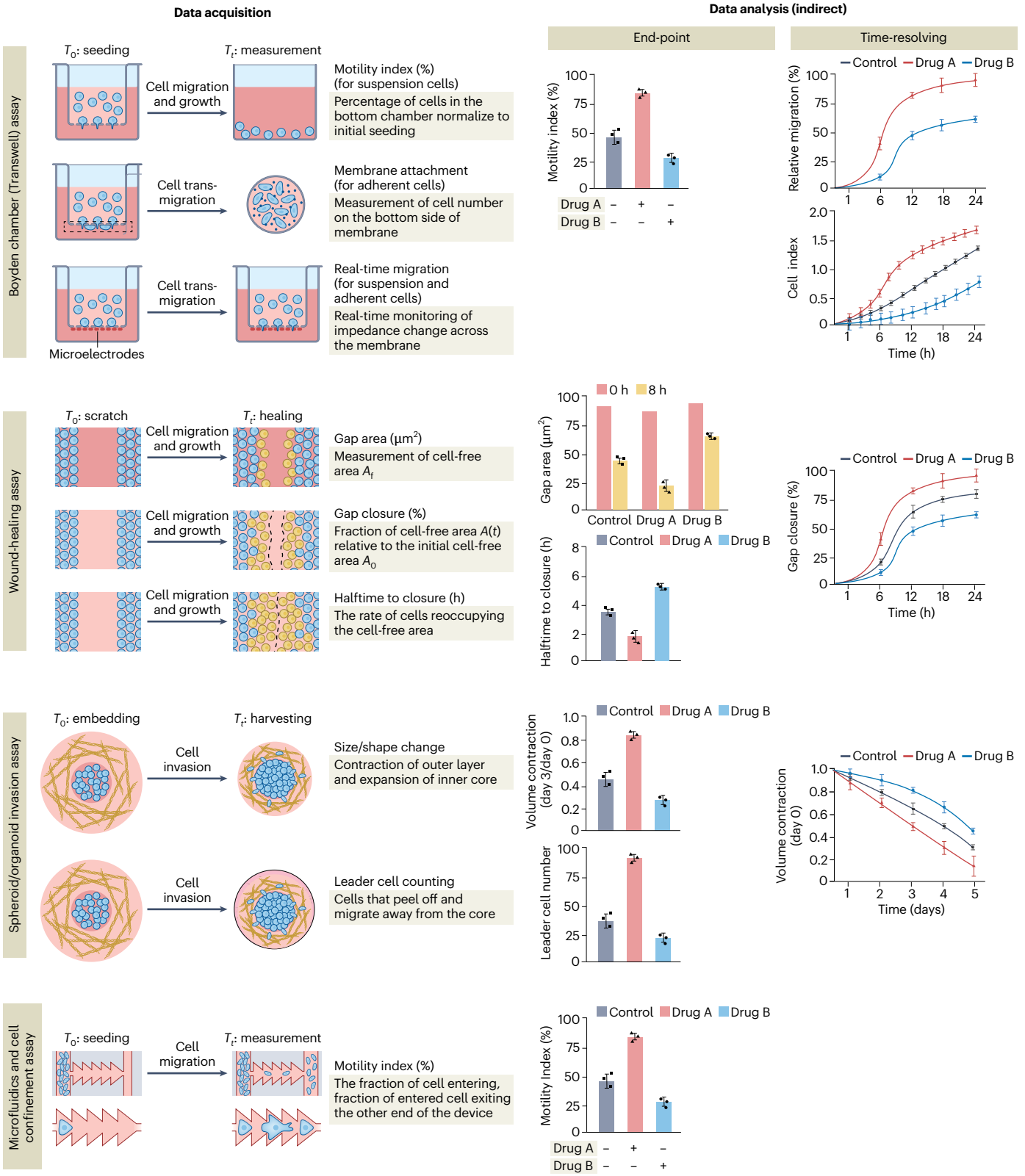

Fig. 4 | Indirect analysis of cell migration via common assays. Indirect measurements entail calculation of the relevant motility index as a proxy of cell migration. Specific motility indices and other migration-related parameters used in different assays are summarized in the data acquisition column, respectively. For the Transwell assay, the number of migrated cells is measured in different compartments of the Boyden chamber for suspension and adherent cells. Acquired motility indices can be plotted either as end points or in a time-resolving manner, as shown in the data analysis column. Created with BioRender.com.

boundary of leading edge (wound edge) closure over time is the most commonly used method to characterize wound-healing assays[96–99]. Images of cell gap area are normally acquired at different time points using light microscopy, typically at a minimum of two time points—the beginning and at a user-defined end point—to compute the fraction of cell-free area A_f relative to the initial size of the cell-free area A_0. In the case where live-cell microscopy equipment is available, including on-stage incubators and microscope stage control, real-time imaging can be performed to compute the wound closure as a function of multiple time points. From these movies, the cell-free area $A(t)$ can be measured using either manual annotations or automated quantification. Armed with the measurement of the cell-free area $A(t)$, key characteristics of migration, such as the average cell migration rate $v_{\text{migration}}$ and halftime to closure $t_{1/2}$, can be computed through curve fitting of equations (7) and (8)[99]:

$$A(t) = A_0 - 2 \times l \times v_{\text{migration}} \times t \tag{7}$$

$$t_{1/2} = A_0/4 \times l \times v_{\text{migration}} \tag{8}$$

Here, l is the length of the cell-free gap in the image (Fig. 4). Automated approaches using image processing approaches have also been developed and implemented to assist with the analysis[98–101]. The impedance-based system has also been developed to speedily (indirectly) measure the changes in gap areas that bypass imaging[34]. In addition to the bulk measurement of wound closure, tracking migration of individual cells in wound-healing assays has been used to assess the motility behavior of individual cells in the moving cell sheet[96,102,103]. In this case, the analysis can follow the direct-migration analysis described in the previous sections. The collective migration behavior in the wound-healing assay can also be characterized using particle image velocimetry[35,104].

The Transwell assay (Boyden chamber assay)

In the Transwell migration assay, cell migration is typically assessed by counting the number of cells, N_{migrated}, that traverse the membrane during a specified incubation period T (Fig. 4). A higher number of cells crossing the membrane indicates greater migration. To count the cells that have migrated across the membrane, various methods are used. Cells can be counted on the underside of the membrane, at the bottom of the wells or in the medium suspension at the bottom, depending on the cell types. Measurement of migrated cells that fall to the bottom chamber is typically used for suspension cells, while measurement on the underside of the membrane is used for adherent cells. According to assay time and cells' migratory potential under various conditions, measurement of adherent cells on the bottom chamber surface should also be included for accurate measurements of cell migration. Various methods can be used to count migrated cells including a hemocytometer, image-based counting or biochemical assays based on ATP hydrolysis or DNA content measurements[105–107]. For image-based counting, brightfield microscopy can be used to count non-labeled cells. Staining techniques such as ultraviolet dyes and DAPI, among others, can enhance the contrast of the cell membrane and assist in cell counting[106,107]. Cells can be counted from the acquired images using software such as ImageJ[106,108]. We note that when counting cells on the bottom side of the membrane, it is necessary to remove cells from the upper side (seeding side) of the membrane through physical swabbing. This step is important due to the close proximity of cells in the upper and lower compartments and the limitations of axial resolution in typical microscope setups to resolve them. The motility index, $\text{MI}_{\text{Transwell}}$, in the Transwell migration assay is usually calculated as the percentage of cells that migrate across the membrane, $N_{\text{migrated}, t=T}$ after period of time T relative to the initial seeding cell count at time 0, $N_{\text{seed}, t=0}$, that is, $\text{MI}_{\text{Transwell}} = N_{\text{cross}, t=T}/N_{\text{seed}, t=0}$. To minimize the confounding effect of cell proliferation, a limited incubation time T is used. Cell counting has traditionally been the primary method of quantification. Impedance-based methods have also been developed for the Transwell migration assay. This method detects changes in impedance across the membrane as cells move through the pores, allowing for continuous monitoring of migrated cells over time[109].

The spheroid/organoid invasion assay

In the spheroid/organoid invasion assay, cell migration is typically assessed indirectly by measuring how far cells spread from the spheroid's initial boundary (Fig. 4). Highly motile cells migrate farther, which is quantified by evaluating the spreading area or the number of cells that have moved beyond the initial spheroid boundary[110–113]. Additionally, the shape of the spreading, such as the number of protrusive fronts, can be used as a characteristic of cell dissemination[114,115]. To analyze these features, the morphology of spheroids/organoids is assessed using imaging-based approaches such as brightfield microscopy or fluorescence microscopy if the cells are fluorescently labeled. While spheroids are inherently three-dimensional structures, cross-sectional 2D images are more typically captured and analyzed. This preference is likely due to the reduced technical challenges associated with volumetric imaging and analysis. Both end-point assays at specific time intervals and dynamic analyses have been used to evaluate cell migration in these assays. Various image processing methods and tools have been developed to segment spheroid contours in images, facilitating the analysis of spheroid/organoid results for both brightfield and fluorescence images[110,116–119].

In addition to indirect analysis, direct analysis by tracking individual cell trajectories can also be used to study migration in spheroid/organoid assays. For such cases, the analysis can refer to the direct-migration analysis sections outlined in this Review. It is important to note that in the spheroid setting, cell migration is often reported in relation to the cells' positions relative to the center of the spheroid core[120,121]. Careful sampling of cells for analysis is essential to avoid sampling bias based on their locations within the spheroid. Furthermore, previous studies have shown that cells in spheroids can follow biased migration patterns as a result of radical stress that aligns peripheral matrix fibers[121]. Therefore, parameters reflecting biased migration features—such as persistence, MSD exponent and speed—provide a more comprehensive characterization of spheroid migration.

The chemotaxis and confined migration assays

Cells typically navigate through complex microenvironments in vivo and must often respond to various physical and chemical perturbations, such as confinement, obstacles and chemical gradients. To study cell migration under diverse microenvironmental cues in a controllable manner, various configurations of microfluidic devices and micropatterning methods have been developed[122–129].

The analysis for this type of assay depends on the device design, for instance, whether cells have to navigate through a series of confined channels or move between pillars of varying spacing. Real-time imaging is implemented to determine the trajectories of individual cells within microfluidic or micropatterned devices[124–127]. In such a case, the direct-migration analysis described above is used to process images and analyze cell migration data. The selection of cell migration features should consider whether the cells undergo biased or random migration, based on the presence of external directional driving forces, such as chemotactic, electrotactic or durotactic gradients within the device[122,128,130–134]. For cells moving inside confining channels, the most common readouts are descriptors of speed or capacity of cells to align their movements with directional cues, including average speed and persistence[124,125,135,136].

Indirect measurements are also used to characterize cell migration in microfluidic assays (Fig. 4). These analyses depend on the specific design of the device used in the assay. For example, in confinement

migration microfluidic designs, counting the number of cells that enter the channels versus those that migrate through to the other side of the channels is often used as a motility index. In chemotaxis-based microfluidic setups, the occurrence of cells migrating a specific distance toward the attractant direction is also commonly used[123,128,137,138].

Outlook

Below, we outline some current limitations and needs for new AI tools, automation and modern data science approaches, which if addressed could enable considerable advances in the analysis and interpretability of cell migration data.

1. A major challenge in analyzing cell migration patterns, especially at the single-cell level, is accurately tracking individual cell positions to map their movement trajectories. This inability to accurately track single cells may stem from a variety of factors, including high local cell density, highly motile cells moving outside the imaging window, poor illumination and noisy images, and cells with low contrast in brightfield images. To provide solutions for these issues, we need to develop fully automated software solutions using deep-learning and AI-based models that (a) are capable of tracking individual cells within high-density environments, (b) utilize adaptive learning to adjust for poor illumination and variations in image quality (noise), (c) account for populations of cells that leave or enter the imaging window, and (d) properly retain the identity of individuals cells even though they may partially overlap or come within close proximity during imaging. Developing solutions that address these points will greatly influence the reliability and scalability of cell migration analyses.
2. There are wide variations in the experimental protocols used to acquire cell migration data. For instance, the total imaging/tracking duration, the rate of image acquisition (the time between consecutive images) and imaging magnification are all determined based on user preferences. While many factors go into selecting experimental parameters (see companion Review[19]), the lack of proper standardization limits the direct integration of disparate cell migration datasets. To enable integration, we need to develop and optimize effective harmonization schemes that can predict the intervening positions of cells that are not physically measured. Some of these approaches include (a) simple interpolations, which work well for predicting intervening positions that are symmetrically spaced (that is, midpoints of measured points), (b) weighted interpolations for non-symmetric intervening positions, which involve adding a directional bias based on subsequent cell positions, and (c) utilizing generative AI models that leverage the spatial and temporal patterns of the cell trajectories to infer intervening positions.
3. Once we have the coordinates of trajectories for large numbers of cells (that is, thousands to tens of thousands of cells, by integrating datasets), we need to extract biological insights. While many cell migration papers rely on insights derived from averaged migration parameters, recent advances in single-cell analysis described above have demonstrated the ability to quantify complex behaviors and phenotypes that define subgroups of cells. However, there is currently a need to develop robust approaches to quantify these behaviors and identify these subgroups of cells. For instance, instead of just plotting the average speed or the average persistence time for each condition, users can compile data matrices with multiple migration parameters (tens to hundreds of migration parameters) for each tracked cell. With this data matrix, users can perform factor analyses or principal component analysis to reduce the dimension and identify orthogonal parameters (that is, independent parameters that contribute most to the observed variance across conditions). Cells can be then clustered based on the orthogonal migration parameters using methods such as *k*-means, unsupervised hierarchical clustering and Leiden clustering, then plotting the individual cells in a low-dimensional representation space, for example, using linear methods such as PCA, or nonlinear methods such as *t*-SNE, UMAP or diffusion maps. While these workflows exist and are routinely used for processing single-cell sequencing data, it is not yet mainstream for cell migration analysis. Optimizing similar approaches of cell migration could improve the biological insights gained from such analysis. Furthermore, in addition to parameterized approaches using user-selected parameters to describe trajectories, deep-learning and AI-based approaches can be leveraged to identify subgroups of cells directly from the videos of cells, their raw coordinates, or treating outlines of cell trajectories as images.
4. Cells in 3D experience different signaling cues that the same cells in 2D, which influence their movements. Measuring cell movements in 3D requires more sophisticated microscopes and imaging workflows. These workflows require *z*-stacks that could limit the temporal resolution of image acquisition due to the amount of time to capture the multiple *z*-stack images and physically moving the stage back to the initial position. To enhance the efficiency of image acquisition and analysis, we need to develop new approaches capable of extracting information of 3D cell movements from single 2D images or sparse sampling of 3D *z*-stacks.
5. Cells exhibit complex biophysical phenotypes across a variety of biological conditions. Cell migration is just one of the cellular phenotypes that may help establish biological insights across conditions. Other relevant cellular phenotypes include cell mechanics (both the stiffness/deformability of cells and the magnitude of traction forces they exert) and morphodynamics (dynamic changes in cell morphology), which is also related to how cells change their shapes to polarize and move. To strengthen the biological insights from these cell phenotypes, we need to develop new analyses capable of simultaneously extracting information on cell migration, morphodynamics and cell mechanics. In the future, we envision approaches where users can simultaneously measure and analyze multiple cell properties to define their cell behaviors. Such approaches will likely require the use and integration of machine learning and other modern data science approaches.
6. Another challenge in analyzing cell migration is establishing functional relationships between cell migration patterns and distinct molecular pathways regulating cell migration. Performing cell migration assays along with single-cell assays (for example, single-cell RNA sequencing) could offer new insights to identify regulators of cell migration. However, we need to develop new approaches to integrate and align single-cell migration data with single-cell sequencing data based on inference mapping. Validation studies can be performed by modulating the gene expression patterns of the identified target genes, for example, based on knockdowns using small interfering RNA of CRISPR. Understanding this relationship could enable the development of trained algorithms to predict how specific molecular/gene expression changes can modulate specific cell migration phenotypes.

Reporting summary

Further information on research design is available in the Nature Portfolio Reporting Summary linked to this article.

References

1. Luster, A. D., Alon, R. & von Andrian, U. H. Immune cell migration in inflammation: present and future therapeutic targets. *Nat. Immunol.* **6**, 1182–1190 (2005.

2. Fowell, D. J. & Kim, M. The spatio-temporal control of effector T cell migration. *Nat. Rev. Immunol.* **21**, 582–596 (2021).
3. Horwitz, R. & Webb, D. Cell migration. *Curr. Biol.* **13**, R756–R759 (2003).
4. Scarpa, E. & Mayor, R. Collective cell migration in development. *J. Cell Biol.* **212**, 143–155 (2016).
5. Kurosaka, S. & Kashina, A. Cell biology of embryonic migration. *Birth Defects Res. C. Embryo Today* **84**, 102–122 (2008).
6. Gurtner, G. C., Werner, S., Barrandon, Y. & Longaker, M. T. Wound repair and regeneration. *Nature* **453**, 314–321 (2008).
7. Arwert, E. N., Hoste, E. & Watt, F. M. Epithelial stem cells, wound healing and cancer. *Nat. Rev. Cancer* **12**, 170–180 (2012).
8. Coulombe, P. A. Wound epithelialization: accelerating the pace of discovery. *J. Invest. Dermatol.* **121**, 219–230 (2003).
9. Aragona, M. et al. Defining stem cell dynamics and migration during wound healing in mouse skin epidermis. *Nat. Commun.* **8**, 14684 (2017).
10. Friedl, P. & Wolf, K. Tumour-cell invasion and migration: diversity and escape mechanisms. *Nat. Rev. Cancer* **3**, 362–374 (2003).
11. Yamaguchi, H., Wyckoff, J. & Condeelis, J. Cell migration in tumors. *Curr. Opin. Cell Biol.* **17**, 559–564 (2005).
12. Castaneda, M., den Hollander, P., Kuburich, N. A., Rosen, J. M. & Mani, S. A. Mechanisms of cancer metastasis. *Semin. Cancer Biol.* **87**, 17–31 (2022).
13. Popper, H. H. Progression and metastasis of lung cancer. *Cancer Metastasis Rev.* **35**, 75–91 (2016).
14. Jones, D. H. et al. Regulation of cancer cell migration and bone metastasis by RANKL. *Nature* **440**, 692–696 (2006).
15. Greten, F. R. & Grivennikov, S. I. Inflammation and cancer: triggers, mechanisms, and consequences. *Immunity* **51**, 27–41 (2019).
16. Fares, J., Fares, M. Y., Khachfe, H. H., Salhab, H. A. & Fares, Y. Molecular principles of metastasis: a hallmark of cancer revisited. *Signal Transduct. Target. Ther.* **5**, 28 (2020).
17. Mackay, C. R. Moving targets: cell migration inhibitors as new anti-inflammatory therapies. *Nat. Immunol.* **9**, 988–998 (2008).
18. Min, H. Y. & Lee, H. Y. Molecular targeted therapy for anticancer treatment. *Exp. Mol. Med.* **54**, 1670–1694 (2022).
19. Du, W. et al. Selecting the optimal cell migration assay: fundamentals and practical guidelines. *Nat. Methods* https://doi.org/10.1038/s41592-025-02890-1 (2025).
20. Fraley, S. I. et al. A distinctive role for focal adhesion proteins in three-dimensional cell motility. *Nat. Cell Biol.* **12**, 598–604 (2010).
21. Wu, P. H., Giri, A. & Wirtz, D. Statistical analysis of cell migration in 3D using the anisotropic persistent random walk model. *Nat. Protoc.* **10**, 517–527 (2015).
22. Giri, A. et al. The Arp2/3 complex mediates multigeneration dendritic protrusions for efficient 3-dimensional cancer cell migration. *FASEB J.* https://doi.org/10.1096/fj.12-224352 (2013).
23. Jayatilaka, H. et al. EB1 and cytoplasmic dynein mediate protrusion dynamics for efficient 3-dimensional cell migration. *FASEB J.* https://doi.org/10.1096/fj.201700444RR (2018).
24. Khatau, S. B. et al. The distinct roles of the nucleus and nucleus-cytoskeleton connections in three-dimensional cell migration. *Sci. Rep.* **2**, 488 (2012).
25. Wu, P. H., Giri, A., Sun, S. X. & Wirtz, D. Three-dimensional cell migration does not follow a random walk. *Proc. Natl Acad. Sci. USA* **111**, 3949–3954 (2014).
26. Stokes, C. L. & Lauffenburger, D. A. Analysis of the roles of microvessel endothelial cell random motility and chemotaxis in angiogenesis. *J. Theor. Biol.* **152**, 377–403 (1991).
27. Stokes, C. L., Lauffenburger, D. A. & Williams, S. K. Migration of individual microvessel endothelial cells: Stochastic model and parameter measurement. *J. Cell Sci.* **99**, 419–430 (1991).
28. Chen, H. C. Boyden chamber assay. *Methods Mol. Biol.* **294**, 15–22 (2005).
29. Justus, C. R., Marie, M. A., Sanderlin, E. J. & Yang, L. V. Transwell in vitro cell migration and invasion assays. *Methods Mol. Biol.* **2644**, 349–359 (2023).
30. Prolo, L. M. et al. Targeted genomic CRISPR-Cas9 screen identifies MAP4K4 as essential for glioblastoma invasion. *Sci. Rep.* **9**, 14020 (2019).
31. Kendirli, A. et al. A genome-wide in vivo CRISPR screen identifies essential regulators of T cell migration to the CNS in a multiple sclerosis model. *Nat. Neurosci.* **26**, 1713–1725 (2023).
32. Ammann, K. R., DeCook, K. J., Li, M. & Slepian, M. J. Migration versus proliferation as contributor to in vitro wound healing of vascular endothelial and smooth muscle cells. *Exp. Cell. Res.* **376**, 58–66 (2019).
33. Grada, A., Otero-Vinas, M., Prieto-Castrillo, F., Obagi, Z. & Falanga, V. Research techniques made simple: analysis of collective cell migration using the wound healing assay. *J. Invest. Dermatol.* **137**, e11–e16 (2017).
34. Keese, C. R., Wegener, J., Walker, S. R. & Giaever, I. Electrical wound-healing assay for cells in vitro. *Proc. Natl Acad. Sci. USA* **101**, 1554–1559 (2004).
35. Riahi, R., Yang, Y., Zhang, D. D. & Wong, P. K. Advances in wound-healing assays for probing collective cell migration. *J. Lab Autom.* **17**, 59–65 (2012).
36. Maška, M. et al. The Cell Tracking Challenge: 10 years of objective benchmarking. *Nat. Methods* **20**, 1010–1020 (2023).
37. Ulman, V. et al. An objective comparison of cell-tracking algorithms. *Nat. Methods* **14**, 1141–1152 (2017).
38. Tinevez, J. Y. et al. TrackMate: an open and extensible platform for single-particle tracking. *Methods* **115**, 80–90 (2017).
39. Uka, A., Tare, A., Polisi, X. & Panci, I. FASTER R-CNN for cell counting in low contrast microscopic images. in *Proceedings of the 2020 International Conference on Computing, Networking, Telecommunications and Engineering Sciences Applications, CoNTESA 2020* 64–69 https://doi.org/10.1109/CONTESA50436.2020.9302852 (2020).
40. Buggenthin, F. et al. An automatic method for robust and fast cell detection in bright field images from high-throughput microscopy. *BMC Bioinformatics* **14**, 297 (2013).
41. Ershov, D. et al. TrackMate 7: integrating state-of-the-art segmentation algorithms into tracking pipelines. *Nat. Methods* **19**, 829–832 (2022).
42. Shim, C. et al. CellTrackVis: interactive browser-based visualization for analyzing cell trajectories and lineages. *BMC Bioinformatics* **24**, 124 (2023).
43. Collins, T. J. ImageJ for microscopy. *Biotechniques* **43**, 25–30 (2007).
44. Schneider, C. A., Rasband, W. S. & Eliceiri, K. W. NIH Image to ImageJ: 25 years of image analysis. *Nat. Methods* **9**, 671–675 (2012).
45. Maity, D. et al. Profiling dynamic patterns of single-cell motility. *Adv. Sci.* **11**, 2400918 (2024).
46. Emami, N., Sedaei, Z. & Ferdousi, R. Computerized cell tracking: current methods, tools and challenges. *Vis. Informatics* **5**, 1–13 (2021).
47. Wu, P. -H. et al. Single-cell morphology encodes metastatic potential. *Sci. Adv.* **6**, eaaw6938 (2020).
48. McQuin, C. et al. CellProfiler 3.0: next-generation image processing for biology. *PLoS Biol* https://doi.org/10.1371/journal.pbio.2005970 (2018).
49. Magidson, V. & Khodjakov, A. Circumventing photodamage in live-cell microscopy. *Methods Cell. Biol.* **114**, 545–560 (2013).
50. Laissue, P. P., Alghamdi, R. A., Tomancak, P., Reynaud, E. G. & Shroff, H. Assessing phototoxicity in live fluorescence imaging. *Nat. Methods* **14**, 657–661 (2017).
51. Icha, J., Weber, M., Waters, J. C. & Norden, C. Phototoxicity in live fluorescence microscopy, and how to avoid it. *BioEssays* **39**, 1700003 (2017).

52. Stringer, C., Wang, T., Michaelos, M. & Pachitariu, M. Cellpose: a generalist algorithm for cellular segmentation. *Nat. Methods* **18**, 100–106 (2020).
53. Copied TextX Schmidt, U., Weigert, M., Broaddus, C. & Myers, G. Cell detection with star-convex polygons. in *Medical Image Computing and Computer Assisted Intervention – MICCAI 2018. MICCAI 2018. Lecture Notes in Computer Science* Vol. 11071, 265–273 (Springer, 2018).
54. Han, K. S. et al. qMAP enabled microanatomical mapping of human skin aging. Preprint at *bioRxiv* https://doi.org/10.1101/2024.04.03.588011 (2024).
55. Cheezum, M. K., Walker, W. F. & Guilford, W. H. Quantitative comparison of algorithms for tracking single fluorescent particles. *Biophys. J.* **81**, 2378–2388 (2001).
56. Wen, C. et al. 3DeeCellTracker, a deep learning-based pipeline for segmenting and tracking cells in 3D time lapse images. *Elife* **10**, e59187 (2021).
57. Miller, M. J., Wei, S. H., Cahalan, M. D. & Parker, I. Autonomous T cell trafficking examined in vivo with intravital two-photon microscopy. *Proc. Natl Acad. Sci. USA* **100**, 2604–2609 (2003).
58. Lau, D. et al. Intravital imaging of adoptive T-cell morphology, mobility and trafficking following immune checkpoint inhibition in a mouse melanoma model. *Front. Immunol.* **11**, 538523 (2020).
59. Wiggins, L. et al. The CellPhe toolkit for cell phenotyping using time-lapse imaging and pattern recognition. *Nat. Commun.* **14**, 1854 (2023).
60. Shannon, M. J., Eisman, S. E., Lowe, A. R., Sloan, T. F. W. & Mace, E. M. cellPLATO – an unsupervised method for identifying cell behaviour in heterogeneous cell trajectory data. *J. Cell Sci.* **137**, jcs261887 (2024).
61. Freckmann, E. C. et al. Traject3D allows label-free identification of distinct co-occurring phenotypes within 3D culture by live imaging. *Nat. Commun.* **13**, 5317 (2022).
62. GitHub. quantixed/TrackMateR: analysis of TrackMate XML outputs in R. https://github.com/quantixed/TrackMateR
63. Wortel, I. M. N. et al. CelltrackR: An R package for fast and flexible analysis of immune cell migration data. *Immunoinformatics* **1–2**, 100003 (2021).
64. Gómez-De-Mariscal, E. et al. CellTracksColab is a platform that enables compilation, analysis, and exploration of cell tracking data. *PLoS Biol.* **22**, e3002740 (2024).
65. Masuzzo, P., Van Troys, M., Ampe, C. & Martens, L. Taking aim at moving targets in computational cell migration. *Trends Cell Biol.* **26**, 88–110 (2016).
66. Meijering, E., Dzyubachyk, O. & Smal, I. Methods for cell and particle tracking. *Methods Enzymol.* **504**, 183–200 (2012).
67. Wu, P. H. et al. Particle tracking microrheology of cancer cells in living subjects. *Mater. Today* **39**, 98–109 (2020).
68. Savin, T. & Doyle, P. S. Static and dynamic errors in particle tracking microrheology. *Biophys. J.* **88**, 623–638 (2005).
69. Wu, P. -H., Arce, S. H., Burney, P. R. & Tseng, Y. A novel approach to high accuracy of video-based microrheology. *Biophys. J.* **96**, 5103–5111 (2009).
70. Metzner, C. et al. Superstatistical analysis and modelling of heterogeneous random walks. *Nat. Commun.* **6**, 7516 (2015).
71. Lan, T. et al. Decomposition of cell activities revealing the role of the cell cycle in driving biofunctional heterogeneity. *Sci. Rep.* **11**, 23431 (2021).
72. Phillip, J. M. et al. Fractional re-distribution among cell motility states during ageing. *Commun. Biol.* **4**, 81 (2021).
73. Lauffenburger, D. A. & Horwitz, A. F. Cell migration: a physically integrated molecular process. *Cell* **84**, 359–369 (1996).
74. Pollard, T. D. & Borisy, G. G. Cellular motility driven by assembly and disassembly of actin filaments. *Cell* **112**, 453–465 (2003).
75. Ridley, A. J. et al. Cell migration: integrating signals from front to back. *Science* **302**, 1704–1709 (2003).
76. Lee, M. H. et al. Mismatch in mechanical and adhesive properties induces pulsating cancer cell migration in epithelial monolayer. *Biophys. J.* **102**, 2731–2741 (2012).
77. Trepat, X. et al. Physical forces during collective cell migration. *Nat. Phys.* **5**, 426–430 (2009).
78. Tambe, D. T. et al. Collective cell guidance by cooperative intercellular forces. *Nat. Mater.* **10**, 469–475 (2011).
79. Dieterich, P., Klages, R., Preuss, R. & Schwab, A. Anomalous dynamics of cell migration. *Proc. Natl Acad. Sci. USA* **105**, 459–463 (2008).
80. Tranquillo, R. T., Lauffenburger, D. A. & Zigmond, S. H. A stochastic model for leukocyte random motility and chemotaxis based on receptor binding fluctuations. *J. Cell Biol.* **106**, 303–309 (1988).
81. Wu, P. -H., Gilkes, D. M. & Wirtz, D. The biophysics of 3D cell migration. *Annu. Rev. Biophys.* **47**, 549–567 (2018).
82. Takagi, H., Sato, M. J., Yanagida, T. & Ueda, M. Functional analysis of spontaneous cell movement under different physiological conditions. *PLoS ONE* **3**, e2648 (2008).
83. Selmeczi, D., Mosler, S., Hagedorn, P. H., Larsen, N. B. & Flyvbjerg, H. Cell motility as persistent random motion: theories from experiments. *Biophys. J.* **89**, 912–931 (2005).
84. Czirok, A., Schlett, K., Madarasz, E. & Vicsek, T. Exponential distribution of locomotion activity in cell cultures. *Phys. Rev. Lett.* **81**, 3038–3041 (1999).
85. Campos, D., Méndez, V. & Llopis, I. Persistent random motion: uncovering cell migration dynamics. *J. Theor. Biol.* **267**, 526–534 (2010).
86. Harris, T. H. et al. Generalized Lévy walks and the role of chemokines in migration of effector $CD8^+$ T cells. *Nature* **486**, 545–548 (2012).
87. Huda, S. et al. Lévy-like movement patterns of metastatic cancer cells revealed in microfabricated systems and implicated in vivo. *Nat. Commun.* **9**, 4539 (2018).
88. Mantegna, R. N. & Stanley, H. E. Stochastic process with ultraslow convergence to a Gaussian: the truncated Lévy flight. *Phys. Rev. Lett.* **73**, 2946 (1994).
89. Godet, I. et al. Fate-mapping post-hypoxic tumor cells reveals a ROS-resistant phenotype that promotes metastasis. *Nat. Commun.* **10**, 4862 (2019).
90. Nair, P. R. et al. MLL1 regulates cytokine-driven cell migration and metastasis. *Sci. Adv.* **10**, eadk0785 (2024).
91. Du, W. et al. High-motility pro-tumorigenic monocytes drive macrophage enrichment in the tumor microenvironment. Preprint at *bioRxiv* https://doi.org/10.1101/2024.07.16.603739 (2024).
92. SenGupta, S., Parent, C. A. & Bear, J. E. The principles of directed cell migration. *Nat. Rev. Mol. Cell Biol.* **22**, 529–547 (2021).
93. Kimmel, J. C., Chang, A. Y., Brack, A. S. & Marshall, W. F. Inferring cell state by quantitative motility analysis reveals a dynamic state system and broken detailed balance. *PLoS Comput. Biol.* **14**, e1005927 (2018).
94. van der Maaten, L. & Hinton, G. Visualizing data using *t*-SNE. *J. Mach. Learn. Res.* **9**, 2579–2605 (2008).
95. McInnes, L., Healy, J. & Melville, J. UMAP: uniform manifold approximation and projection for dimension reduction. Preprint at https://arxiv.org/abs/1802.03426 (2018).
96. Ascione, F. et al. Comparison between fibroblast wound healing and cell random migration assays in vitro. *Exp. Cell. Res.* **347**, 123–132 (2016).
97. Tremel, A. et al. Cell migration and proliferation during monolayer formation and wound healing. *Chem. Eng. Sci.* **64**, 247–253 (2009).
98. Zordan, M. D., Mill, C. P., Riese, D. J. & Leary, J. F. A high throughput, interactive imaging, bright-field wound healing assay. *Cytometry A* **79**, 227–232 (2011).

99. Jonkman, J. E. N. et al. An introduction to the wound healing assay using live-cell microscopy. *Cell Adh. Migr.* **8**, 440–451 (2014).
100. Kauanova, S., Urazbayev, A. & Vorobjev, I. The frequent sampling of wound scratch assay reveals the 'opportunity' window for quantitative evaluation of cell motility-impeding drugs. *Front. Cell Dev. Biol.* **9**, 640972 (2021).
101. Main, K. A., Mikelis, C. M. & Doçi, C. L. In vitro wound healing assays to investigate epidermal migration. *Methods Mol. Biol.* **2109**, 147–154 (2020).
102. Chung, H. H., Bellefeuille, S. D., Miller, H. N. & Gaborski, T. R. Extended live-tracking and quantitative characterization of wound healing and cell migration with SiR-Hoechst. *Exp. Cell. Res.* **373**, 198–210 (2018).
103. Bise, R., Kanade, T., Yin, Z. & Huh, S. Il. Automatic cell tracking applied to analysis of cell migration in wound healing assay. *Annu. Int. Conf. IEEE Eng. Med. Biol. Soc.* **2011**, 6174–6179 (2011).
104. Poujade, M. et al. Collective migration of an epithelial monolayer in response to a model wound. *Proc. Natl Acad. Sci. USA* **104**, 15988–15993 (2007).
105. Hulkower, K. I. & Herber, R. L. Cell migration and invasion assays as tools for drug discovery. *Pharmaceutics* **3**, 107–124 (2011).
106. Pijuan, J. et al. In vitro cell migration, invasion, and adhesion assays: from cell imaging to data analysis. *Front. Cell Dev. Biol.* **7**, 449183 (2019).
107. Justus, C. R., Leffler, N., Ruiz-Echevarria, M. & Yang, L. V. In vitro cell migration and invasion assays. *J. Vis. Exp.* https://doi.org/10.3791/51046 (2014).
108. O'brien, J., Hayder, H. & Peng, C. Automated quantification and analysis of cell counting procedures using ImageJ plugins. *J. Vis. Exp.* **2016**, e54719 (2016).
109. Bird, C. & Kirstein, S. Real-time, label-free monitoring of cellular invasion and migration with the xCELLigence system. *Nat. Methods* https://doi.org/10.1038/nmeth.f.263 (2009).
110. Vinci, M. et al. Advances in establishment and analysis of three-dimensional tumor spheroid-based functional assays for target validation and drug evaluation. *BMC Biol.* **10**, 29 (2012).
111. Russo, G. C. et al. E-cadherin interacts with EGFR resulting in hyper-activation of ERK in multiple models of breast cancer. *Oncogene* **43**, 1445–1462 (2024).
112. Lee, M. H. et al. Multi-compartment tumor organoids. *Mater. Today* **61**, 104–116 (2022).
113. Puls, T. J. et al. Development of a novel 3D tumor-tissue invasion model for high-throughput, high-content phenotypic drug screening. *Sci. Rep.* **8**, 13039 (2018).
114. Randriamanantsoa, S. et al. Spatiotemporal dynamics of self-organized branching in pancreas-derived organoids. *Nat. Commun.* **13**, 5219 (2022).
115. Goranci-Buzhala, G. et al. Rapid and efficient invasion assay of glioblastoma in human brain organoids. *Cell Rep.* **31**, 107738 (2020).
116. Friedrich, J., Seidel, C., Ebner, R. & Kunz-Schughart, L. A. Spheroid-based drug screen: considerations and practical approach. *Nat. Protoc.* **4**, 309–324 (2009).
117. Vinci, M., Box, C. & Eccles, S. A. Three-dimensional (3D) tumor spheroid invasion assay. *J. Vis. Exp.* **2015**, 52686 (2015).
118. Chen, Z. et al. Automated evaluation of tumor spheroid behavior in 3D culture using deep learning-based recognition. *Biomaterials* **272**, 120770 (2021).
119. Heiss, J. & Tavana, H. Automated analysis of extracellular matrix invasion of cancer cells from tumor spheroids. *ACS Meas. Sci. Au* **4**, 260–266 (2024).
120. Konen, J. et al. Image-guided genomics of phenotypically heterogeneous populations reveals vascular signalling during symbiotic collective cancer invasion. *Nat. Commun.* **8**, 15078 (2017).
121. Valencia, A. M. J. et al. Collective cancer cell invasion induced by coordinated contractile stresses. *Oncotarget* **6**, 43438–43451 (2015).
122. Kim, B. J. & Wu, M. Microfluidics for mammalian cell chemotaxis. *Ann. Biomed. Eng.* **40**, 1316–1327 (2012).
123. Chen, Y. C. et al. Single-cell migration chip for chemotaxis-based microfluidic selection of heterogeneous cell populations. *Sci. Rep.* **5**, 9980 (2015).
124. Yankaskas, C. L. et al. A microfluidic assay for the quantification of the metastatic propensity of breast cancer specimens. *Nat. Biomed. Eng.* **3**, 452–465 (2019).
125. Stroka, K. M. et al. Water permeation drives tumor cell migration in confined microenvironments. *Cell* **157**, 611–623 (2014).
126. Jiang, X., Bruzewicz, D. A., Wong, A. P., Piel, M. & Whitesides, G. M. Directing cell migration with asymmetric micropatterns. *Proc. Natl Acad. Sci. USA* **102**, 975–978 (2005).
127. Bhattacharya, S. et al. A high-throughput microfabricated platform for rapid quantification of metastatic potential. *Sci. Adv.* **10**, eadk0015 (2024).
128. Wu, J., Wu, X. & Lin, F. Recent developments in microfluidics-based chemotaxis studies. *Lab Chip* **13**, 2484–2499 (2013).
129. Sackmann, E. K., Fulton, A. L. & Beebe, D. J. The present and future role of microfluidics in biomedical research. *Nature* **507**, 181–189 (2014).
130. Li, J. & Lin, F. Microfluidic devices for studying chemotaxis and electrotaxis. *Trends Cell Biol.* **21**, 489–497 (2011).
131. Sun, Y. S. Studying electrotaxis in microfluidic devices. *Sensors* **17**, 2048 (2017).
132. Li, Y. et al. Cell migration microfluidics for electrotaxis-based heterogeneity study of lung cancer cells. *Biosens. Bioelectron.* **89**, 837–845 (2017).
133. Sunyer, R. & Trepat, X. Durotaxis. *Curr. Biol.* **30**, R383–R387 (2020).
134. Style, R. W. et al. Patterning droplets with durotaxis. *Proc. Natl Acad. Sci. USA* **110**, 12541–12544 (2013).
135. Fanfone, D. et al. Confined migration promotes cancer metastasis through resistance to anoikis and increased invasiveness. *Elife* **11**, e73150 (2022).
136. Paul, C. D., Mistriotis, P. & Konstantopoulos, K. Cancer cell motility: lessons from migration in confined spaces. *Nat. Rev. Cancer* **17**, 131–140 (2016).
137. Zengel, P. et al. μ-slide chemotaxis: a new chamber for long-term chemotaxis studies. *BMC Cell Biol.* **12**, 21 (2011).
138. Lambert, B. S. et al. A microfluidics-based in situ chemotaxis assay to study the behaviour of aquatic microbial communities. *Nat. Microbiol.* **2**, 1344–1349 (2017).
139. Sacan, A., Ferhatosmanoglu, H. & Coskun, H. CellTrack: an open-source software for cell tracking and motility analysis. *Bioinformatics* **24**, 1647–1649 (2008).
140. Hu, T., Xu, S., Wei, L., Zhang, X. & Wang, X. CellTracker: an automated toolbox for single-cell segmentation and tracking of time-lapse microscopy images. *Bioinformatics* **37**, 285–287 (2021).
141. Kamentsky, L. et al. Improved structure, function and compatibility for CellProfiler: modular high-throughput image analysis software. *Bioinformatics* **27**, 1179–1180 (2011).
142. Stirling, D. R. et al. CellProfiler 4: improvements in speed, utility and usability. *BMC Bioinformatics* **22**, 433 (2021).
143. Pachitariu, M. & Stringer, C. Cellpose 2.0: how to train your own model. *Nat. Methods* **19**, 1634–1641 (2022).
144. Aragaki, H., Ogoh, K., Kondo, Y. & Aoki, K. LIM Tracker: a software package for cell tracking and analysis with advanced interactivity. *Sci. Rep.* **12**, 2702 (2022).
145. Lugagne, J. -B., Lin, H. & Dunlop, M. J. DeLTA: automated cell segmentation, tracking, and lineage reconstruction using deep learning. *PLoS Comput. Biol.* **16**, e1007673 (2020).
146. Zhao, Y. et al. HFM-Tracker: a cell tracking algorithm based on hybrid feature matching. *Analyst* **149**, 2629–2636 (2024).

147. Deforet, M. et al. Automated velocity mapping of migrating cell populations (AVeMap). *Nat. Methods* **9**, 1081–1083 (2012).
148. Amat, F. et al. Fast, accurate reconstruction of cell lineages from large-scale fluorescence microscopy data. *Nat. Methods* **11**, 951–958 (2014).
149. Cordelières, F. P. et al. Automated cell tracking and analysis in phase-contrast videos (iTrack4U): development of Java software based on combined mean-shift processes. *PLoS ONE* **8**, e81266 (2013).
150. Masuzzo, P. et al. CellMissy: a tool for management, storage and analysis of cell migration data produced in wound healing-like assays. *Bioinformatics* **29**, 2661–2663 (2013).
151. Gebäck, T., Schulz, M. M. P., Koumoutsakos, P. & Detmar, M. TScratch: a novel and simple software tool for automated analysis of monolayer wound healing assays. *Biotechniques* **46**, 265–274 (2009).
152. Garcia-Fossa, F., Gaal, V. & de Jesus, M. B. PyScratch: an ease of use tool for analysis of scratch assays. *Comput. Methods Programs Biomed.* **193**, 105476 (2020).
153. Cortesi, M., Pasini, A., Tesei, A. & Giordano, E. AIM: a computational tool for the automatic quantification of scratch wound healing assays. *Appl. Sci.* **7**, 1237 (2017).
154. Li, X., Yang, H., Huang, H. & Zhu, T. CELLCOUNTER: novel open-source software for counting cell migration and invasion in vitro. *Biomed. Res. Int.* **2014**, 863564 (2014).
155. Cortesi, M. et al. I-AbACUS: a reliable software tool for the semi-automatic analysis of invasion and migration Transwell assays. *Sci. Rep.* **8**, 3814 (2018).
156. Chen, W. et al. High-throughput image analysis of tumor spheroids: a user-friendly software application to measure the size of spheroids automatically and accurately. *J. Vis. Exp.* https://doi.org/10.3791/51639 (2014).
157. Piccinini, F. AnaSP: a software suite for automatic image analysis of multicellular spheroids. *Comput. Methods Prog. Biomed.* **119**, 43–52 (2015).
158. Akshay, A. et al. SpheroScan: a user-friendly deep learning tool for spheroid image analysis. *Gigascience* **12**, giad082 (2022).
159. Park, T. et al. Development of a deep learning based image processing tool for enhanced organoid analysis. *Sci. Rep.* **13**, 19841 (2023).
160. Matthews, J. M. et al. OrganoID: a versatile deep learning platform for tracking and analysis of single-organoid dynamics. *PLoS Comput. Biol.* **18**, e1010584 (2022).

Acknowledgements

We acknowledge the following sources of support: U54AR081774 (to D.W.), U54CA268083 (to D.W.), R01CA300052 (to D.W.), UG3CA275681 (to P.-H.W.) and UH3CA275681 (to P.-H.W.), all from the National Cancer Institute; R35-GM157099 (to J.M.P.) from the National Institute of General Medical Sciences; and an American Federation for Aging Research Glenn Foundation Junior Faculty Award (to J.M.P.).

Author contributions

D.W., P.-H.W. and J.M.P. conceived the outline. P.-H.W., J.M.P., W.D., A.F., P.R.N. and D.W. wrote the paper.

Competing interests

The authors declare no competing interests.

Additional information

Supplementary information The online version contains supplementary material available at https://doi.org/10.1038/s41592-025-02935-5.

Correspondence and requests for materials should be addressed to Pei-Hsun Wu, Jude M. Phillip or Denis Wirtz.

Peer review information *Nature Methods* thanks Li Yang, and the other, anonymous, reviewer(s) for their contribution to the peer review of this work. Primary Handling Editor: Rita Strack, in collaboration with the *Nature Methods* team.

nature portfolio

Corresponding author(s): Denis Wirtz

Last updated by author(s): Jul 7, 2025

Reporting Summary

Nature Portfolio wishes to improve the reproducibility of the work that we publish. This form provides structure for consistency and transparency in reporting. For further information on Nature Portfolio policies, see our Editorial Policies and the Editorial Policy Checklist.

Statistics

For all statistical analyses, confirm that the following items are present in the figure legend, table legend, main text, or Methods section.

n/a	Confirmed
☒	☐ The exact sample size (*n*) for each experimental group/condition, given as a discrete number and unit of measurement
☒	☐ A statement on whether measurements were taken from distinct samples or whether the same sample was measured repeatedly
☒	☐ The statistical test(s) used AND whether they are one- or two-sided *Only common tests should be described solely by name; describe more complex techniques in the Methods section.*
☒	☐ A description of all covariates tested
☒	☐ A description of any assumptions or corrections, such as tests of normality and adjustment for multiple comparisons
☒	☐ A full description of the statistical parameters including central tendency (e.g. means) or other basic estimates (e.g. regression coefficient) AND variation (e.g. standard deviation) or associated estimates of uncertainty (e.g. confidence intervals)
☒	☐ For null hypothesis testing, the test statistic (e.g. *F*, *t*, *r*) with confidence intervals, effect sizes, degrees of freedom and *P* value noted *Give P values as exact values whenever suitable.*
☒	☐ For Bayesian analysis, information on the choice of priors and Markov chain Monte Carlo settings
☒	☐ For hierarchical and complex designs, identification of the appropriate level for tests and full reporting of outcomes
☒	☐ Estimates of effect sizes (e.g. Cohen's *d*, Pearson's *r*), indicating how they were calculated

Our web collection on statistics for biologists contains articles on many of the points above.

Software and code

Policy information about availability of computer code

Data collection	Not Applicable
Data analysis	BioRender was used to generate all illustration figures in this review

For manuscripts utilizing custom algorithms or software that are central to the research but not yet described in published literature, software must be made available to editors and reviewers. We strongly encourage code deposition in a community repository (e.g. GitHub). See the Nature Portfolio guidelines for submitting code & software for further information.

Data

Policy information about availability of data

All manuscripts must include a data availability statement. This statement should provide the following information, where applicable:

- Accession codes, unique identifiers, or web links for publicly available datasets
- A description of any restrictions on data availability
- For clinical datasets or third party data, please ensure that the statement adheres to our policy

No new datasets were used in this review.

Human research participants

Policy information about studies involving human research participants and Sex and Gender in Research.

Reporting on sex and gender	Not Applicable
Population characteristics	Not Applicable
Recruitment	Not Applicable
Ethics oversight	Not Applicable

Note that full information on the approval of the study protocol must also be provided in the manuscript.

Field-specific reporting

Please select the one below that is the best fit for your research. If you are not sure, read the appropriate sections before making your selection.

☒ Life sciences ☐ Behavioural & social sciences ☐ Ecological, evolutionary & environmental sciences

For a reference copy of the document with all sections, see nature.com/documents/nr-reporting-summary-flat.pdf

Life sciences study design

All studies must disclose on these points even when the disclosure is negative.

Sample size	166 studies (research articles and reviews) were evaluated in a systematic review analysis.
Data exclusions	Studies that used migration assays were included (the majority of studies included were peer-reviewed; a few preprints were also included due to their significance). Studies were excluded when they were not primarily in English.
Replication	Not Applicable
Randomization	Not Applicable
Blinding	Not Applicable

Reporting for specific materials, systems and methods

We require information from authors about some types of materials, experimental systems and methods used in many studies. Here, indicate whether each material, system or method listed is relevant to your study. If you are not sure if a list item applies to your research, read the appropriate section before selecting a response.

Materials & experimental systems

n/a	Involved in the study
☒	☐ Antibodies
☒	☐ Eukaryotic cell lines
☒	☐ Palaeontology and archaeology
☒	☐ Animals and other organisms
☒	☐ Clinical data
☒	☐ Dual use research of concern

Methods

n/a	Involved in the study
☒	☐ ChIP-seq
☒	☐ Flow cytometry
☒	☐ MRI-based neuroimaging